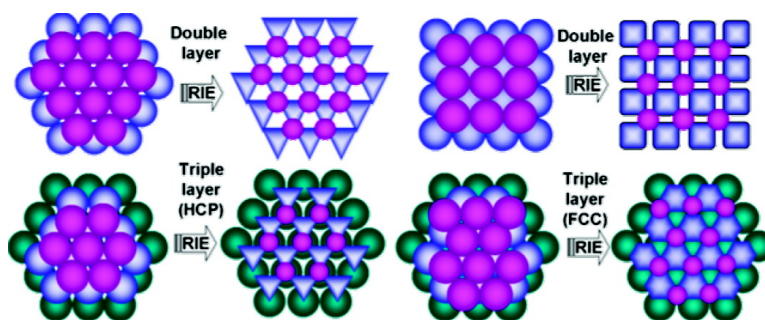


Colloidal Lithographic Nanopatterning via Reactive Ion Etching

Dae-Geun Choi, Hyung Kyun Yu, Se Gyu Jang, and Seung-Man Yang

J. Am. Chem. Soc., **2004**, 126 (22), 7019-7025 • DOI: 10.1021/ja0319083 • Publication Date (Web): 14 May 2004

Downloaded from <http://pubs.acs.org> on March 31, 2009



More About This Article

Additional resources and features associated with this article are available within the HTML version:

- Supporting Information
- Links to the 12 articles that cite this article, as of the time of this article download
- Access to high resolution figures
- Links to articles and content related to this article
- Copyright permission to reproduce figures and/or text from this article

[View the Full Text HTML](#)



Colloidal Lithographic Nanopatterning via Reactive Ion Etching

Dae-Geun Choi, Hyung Kyun Yu, Se Gyu Jang, and Seung-Man Yang*

Contribution from the Department of Chemical and Biomolecular Engineering, Korea Advanced Institute of Science and Technology, 373-1, Guseong-dong, Yuseong-gu, Daejeon 305-701 Korea

Received December 23, 2003; E-mail: smyang@kaist.ac.kr

Abstract: We report here a novel colloidal lithographic approach to the fabrication of nonspherical colloidal particle arrays with a long-range order by selective reactive ion etching (RIE) of multilayered spherical colloidal particles. First, layered colloidal crystals with different crystal structures (or orientations) were self-organized onto substrates. Then, during the RIE, the upper layer in the colloidal multilayer acted as a mask for the lower layer and the resulting anisotropic etching created nonspherical particle arrays and new patterns. The new patterns have shapes that are different from the original as a result of the relative shadowing of the RIE process by the top layer and the lower layers. The shape and size of the particles and patterns were dependent on the crystal orientation relative to the etchant flow, the number of colloidal layers, and the RIE conditions. The various colloidal patterns can be used as masks for two-dimensional (2-D) nanopatterns. In addition, the resulting nonspherical particles can be used as novel building blocks for colloidal photonic crystals.

Introduction

The fabrication of colloidal particle arrays in 2-D or 3-D arrangements has potential applications to biochips and biosensors,¹ to electronic devices,² and as templates for designed nanostructures.³ In particular, patterned arrays consisting of nonspherical lattices are of practical significance in the fabrication of metal dot arrays for magnetic memory devices and photonic crystals for optical devices. This interest derives from the fact that the remanence of magnetic metal dots and optical properties of dielectric particle arrays are sensitive to particle size and shape.^{4–6}

Thus far, most studies in these areas have used spherical particles because their monodisperse sample can be easily prepared by various synthetic routes.⁷ While spherical particles can represent the simplest form of building blocks that can be self-organized into ordered structures, they are not ideal for all types of fundamental research or practical applications that

involve the use of colloidal particles.⁸ Furthermore, in applications that require periodic structures, nonspherical particles can provide new types of functionalities that would not be given by spherical particles.⁹ For example, photonic crystals of nonspherical lattices can break the symmetry-induced degeneracy of polarization modes and thus achieve complete photonic band gaps in cases that otherwise would exhibit only stop bands in limited directions.⁵ Recently, ellipsoidal or peanutlike particles or colloidal clusters such as dimers and tetramers have been fabricated by indirect methods that use geometric confinement or viscoelastic deformation of spherical colloidal particles.^{7–10} However, it is difficult to make self-assembled structures with a long-range order using these separate building blocks of nonspherical asymmetric shape.

Meanwhile, various nanofabrication techniques such as soft lithography,¹¹ and laser interference lithography,¹² as well as E-beam and X-ray lithography,¹³ have been used for 2-D patterned surfaces. Although these lithographic techniques based on a “top-down approach” are useful in pattern fabrication, cost and process considerations limit their usefulness.¹⁴ Self-assembly techniques that use chemical or physical driving forces based on a “bottom-up approach” are an alternative; these techniques

- (1) (a) Hagleitner, C.; Hierlemann, A.; Lange, D.; Kummer, A.; Kerness, N.; Brand, O.; Baltes, H. *Nature* **2001**, *414*, 293. (b) Velev, O. D.; Jede, T. A.; Lobo, R. F.; Lenhoff, A. M. *Nature* **1997**, *389*, 447. (c) Shi, H. Q.; Tsai, W. B.; Garrison, M. D.; Ferrari S.; Ratner, B. D. *Nature* **1999**, *398*, 593. (d) Cui, Y.; Wei, Q. Q.; Park H. K.; Leiber, C. M. *Science* **2001**, *293*, 1289.
- (2) (a) Xia, Y.; Kim, E.; Zhao, X. M.; Rogers, J. A.; Prentiss M.; Whitesides, G. M. *Science* **1996**, *273*, 347. (b) Veinot, J. G. C.; Yan, H.; Smith, S. M.; Cui, J.; Huang, Q.; Marks, T. J. *Nano Lett.* **2002**, *2*, 333.
- (3) (a) Jiang, P.; Bertone, J. F.; Colvin, V. L. *Science* **2001**, *291*, 453. (b) Yi, D. K.; Yoo S. J.; Kim, D.-Y. *Nano Lett.* **2002**, *2*, 1101
- (4) (a) Stuart, H. R.; Hall, D. G. *Appl. Phys. Lett.* **1996**, *69*, 2327. (b) Chou, S. Y.; Wei, M. S.; Krauss, P. R.; Fischer, P. B. *J. Appl. Phys.* **1994**, *76*, 6673.
- (5) (a) Imhof, A.; Pine, D. J. *Nature* **1997**, *389*, 948. (b) Velev, O. D.; Lenhoff, A. M.; Kaler, E. W. *Science* **2000**, *287*, 2240. (c) Yi, G.-R.; Moon, J. H.; Manoharan, V. N.; Pine, D. J.; Yang, S.-M. *J. Am. Chem. Soc.* **2002**, *124*, 13354. (d) Zhong, Z. Y.; Gates B.; Xia, Y. N. *Langmuir* **2000**, *16*, 10369.
- (6) (a) Moroz, A. *Phys. Rev. Lett.* **1999**, *83*, 5274. (b) Jiang, P.; Bertone, J. F.; Colvin, V. L. *Science* **2001**, *291*, 453.
- (7) Larsen, A. E.; Grier, D. G. *Nature* **1997**, *385*, 230.

- (8) Yin, Y.; Lu, Y.; Xia, Y. *J. Am. Chem. Soc.* **2001**, *123*, 771.
- (9) Xia, Y.; Gates, B.; Yin, Y.; Lu, Y. *Adv. Mater.* **2000**, *12*, 693.
- (10) (a) Lu, Y.; Yin, Y.; Xia, Y. *Adv. Mater.* **2001**, *13*, 415. (b) Manoharan, V. N.; Elssesser, M. T.; Pine, D. J. *Science* **2003**, *301*, 483.
- (11) (a) Xia, Y. N.; Whitesides, G. M. *Angew. Chem., Int. Ed.* **1998**, *37*, 551. (b) Chou, S. Y.; Krauss, P. R.; Renstrom, P. J. *Science* **1996**, *272*, 85.
- (12) (a) Shoji, S.; Kawata, S. *Appl. Phys. Lett.* **2000**, *76*, 2668. (b) Campbell, M.; Sharp, D. N.; Harrison, M. T.; Denning R. G.; Turberfield, A. J. *Nature* **2000**, *404*, 53.
- (13) Todorovic, M.; Schultz, S.; Wong, J.; Scherer, A. *Appl. Phys. Lett.* **1999**, *74*, 2516.
- (14) (a) Chou, S. Y.; Krauss, P. R.; Renstrom, P. J. *J. Vac. Sci. Technol., B* **1996**, *14*, 4129. (b) Albrecht, M.; Rettner, C. T.; Anders, S.; Thomson, T.; Best, M. E.; Moser, A.; Terris, B. D. *J. Appl. Phys.* **2002**, *91*, 6845.

allow simple control of the pattern size and low-cost parallel processes that use porous alumina,¹⁵ block copolymers,¹⁶ and colloidal particles.¹⁷ Specifically, well-organized 2-D particle arrays are important in applications of stamps for soft lithography,¹⁸ microlenses,¹⁹ carbon nanotube arrays,²⁰ and colloidal lithography (CL); these applications use colloidal arrays as lithographic masks or templates to fabricate nanostructures.²¹ CL has the advantage of being an inexpensive, inherently parallel, high-throughput nanofabrication technique.²¹ Mainly single and double layers of colloidal particles have been used as masks or templates for patterned polymers and metals. In these cases, the interstices between particles were used as a space for the infiltration of new materials. A close-packed colloidal assembly usually forms a triangular-shaped interstice in the single layer or a hexagonal-shaped interstice in the double layer. The in-plane diameters of the interstices in close-packed layers of colloidal spheres of diameter D are usually given by $a_{SL} = 0.233D$ for single layers and $a_{DL} = 0.1555D$ for double layers.²¹

One disadvantage of CL that limits the application of the CL technique is its ineffectiveness in tuning the size and shape of a structure. The size and shape of a nanostructure are usually dependent on the original particle size. Recently, however, several techniques for controlling the size and shape of nanostructures have been suggested, including angle-resolved deposition,²² control of deposition thickness, and dry-etching conditions.²³ These methods use the close-packed colloidal layers with the constant size of the interstices between particles as masks to control the size and shape of a nanostructure.

Meanwhile, reactive ion (plasma) etching (RIE) has been used to control the surface morphology and roughness and to enhance surface hydrophilicity in polymeric and biological applications.^{24,25a} Recently, RIE was used to fabricate polymeric nanofibrillar surfaces²⁵ and patterned structures using colloidal single layers²⁶ and double layers.²⁷ However, RIE of the colloidal layers is limited either to the simple size-reduction of colloidal spheres by oxygen RIE or to 2-D pattern formation using double-layered colloidal sphere-assembly. As such, research on the control of nanostructures remains a challenge, and new techniques are needed.

Here, we report a simple and novel approach to the fabrication of 2-D or 3-D arrays of nonspherical colloidal particles of various shapes through CL. Specifically, we created well-organized layers of nonspherical colloidal particles by using the anisotropic RIE of the spherical polymer latexes that were stacked layer by layer, with the top layer acting as a mask. Our approach has several advantages. First, binary (or ternary) colloidal particle arrays with different sizes and shapes can be easily fabricated from identically sized spherical particles.²⁸ Second, the size and shape of the resulting nonspherical particles and interstices in the colloidal layer can be easily controlled by the crystal orientation, the number of colloidal layers, and the RIE conditions. Finally, an exact assessment of a face-centered cubic (fcc) crystal structure or a hexagonal-closed packing (hcp) crystal structure is possible by simple and direct SEM of the CL patterned structures. Such assessment is important in the research areas of colloidal science and photonic crystals. This article is unique and significant in that it reports the results of CL when either the (100) or (111) plane of fcc or hcp colloidal crystals is exposed to an etchant flow under various RIE conditions. The resulting particle arrays show complicated structures that cannot otherwise be produced. The structure of nonspherical colloidal arrays could be used as templates or masks for subsequent deposition of magnetic metal dots or etching processes. In addition, the resulting nonspherical particles can be used as novel building blocks for colloidal photonic crystals.

Experimental Section

A schematic of our fabrication strategy of binary and ternary particle arrays with nonspherical building blocks is shown in Figure 1. First, aqueous colloidal polystyrene (PS) spheres with a diameter of 1.01 μm were purchased from Magsphere, and PS spheres with a diameter of 200 nm were synthesized by emulsifier-free emulsion polymerization.^{29,30} In emulsion polymerization, we used potassium persulfate as an initiator to form the initiating radicals that were soluble in aqueous phase and able to bind to hydrophobic styrene monomers. In the early stage of polymerization, the short growing chain was amphiphilic, but growing radicals in water lost their solubility owing to the increasing hydrophobicity with increasing chain length. Thus, the hydrophilic parts of precipitating chains tended to contact with the aqueous phase while the hydrophobic chains were likely to aggregate with each other, which resulted in the formation of spherical organic microspheres with hydrophilic surface species. The hydrophilicity of PS surface was increased by adding a small amount of a hydrophilic comonomer of acrylic acid or sodium styrene sulfonate which was copolymerized with hydrophobic styrene monomer. Due to the hydrophilic surfaces, the PS beads were dispersed readily in water. The concentrations of the PS suspensions were 0.7 wt % to 1.0 wt % for the 1.01 μm PS bead and 0.07 wt % to 0.1 wt % for the 200 nm PS bead.

A colloidal multilayer of PS beads was produced by raising either a clean flat glass substrate or a replica-molded polyurethane (PU) substrate with V-shaped grooves, both of which had been previously immersed in the PS suspension. For the replica molding of PU, we used a V-shaped diffraction grating (TGG01, MicroMasch) as a master mold. The angle between the edges of the V-shaped groove was 70°. All of the glass substrates were cleaned using toluene, acetone, ethanol, and distilled water in an ultrasonic bath (Branson 2510), and both the cleaned glass and the PU substrates were exposed to O₂ plasma to

- (15) (a) Masuda, H.; Fukuda, K. *Science* **1995**, *268*, 1466. (b) Choi, J.; Wehrspohn, R. B.; Gösele, U. *Adv. Mater.* **2003**, *15*, 1531.
- (16) (a) Black, C. T.; Guarini, K. W.; Milkove, K. R.; Baker, S. M.; Tuominen, M. T.; Russell, T. P. *Appl. Phys. Lett.* **2001**, *79*, 409. (b) Zhao, D.; Feng, J.; Huo, Q.; Melosh, N.; Fredrickson, G. H.; Chemelka, B. F.; Stucky, G. D. *Science* **1998**, *279*, 548.
- (17) Chen, X.; Chen, Z.; Fu, N.; Lu, G.; Yang, B. *Adv. Mater.* **2003**, *15*, 1413.
- (18) Kuo, C.-W.; Shiu, J.-Y.; Cho, Y.-H.; Chen, P. *Adv. Mater.* **2003**, *15*, 1065.
- (19) Wu, M.-H.; Whitesides, G. M. *Appl. Phys. Lett.* **2001**, *78*, 2273.
- (20) Hung, Z. P.; Carhahan, D. L.; Rybcynski, J.; Giersig, M.; Sennett, M.; Wang, D. Z.; Wen, J. G.; Kempa, K.; Ren, Z. F. *Appl. Phys. Lett.* **2003**, *82*, 460.
- (21) (a) Haynes, C. L.; Van Duyne, R. P. *J. Phys. Chem. B* **2001**, *105*, 5599. (b) Hulteen, J. C.; Treichel, D. A.; Smith, M. T.; Duval, M. L.; Jensen, T. R.; Van Duyne, R. P. *J. Phys. Chem. B* **1999**, *103*, 3854. (c) Yi, D. K.; Kim, D.-Y. *Chem. Commun.* **2003**, 982.
- (22) Haynes, C. L.; McFarland, A. D.; Smith, M. T.; Hulteen, J. C.; Van Duyne, R. P. *J. Phys. Chem. B* **2002**, *106*, 1898.
- (23) (a) Kuo, C.-W.; Shiu, J.-Y.; Chen, P. *Chem. Mater.* **2003**, *15*, 2917. (b) Kuo, C.-W.; Shiu, J.-Y.; Chen, P.; Somorjai, G. A. *J. Phys. Chem. B* **2003**, *107*, 9950.
- (24) (a) Egitto, F. D.; Matienzo, L. J. *IBM J. Res. Dev.* **1994**, *38*, 423. (b) Nakamatsu, J.; Delgado-Aparicio, L. F.; Da Silva, R.; Soberon, F. *J. Adhes. Sci. Technol.* **1999**, *13*, 753. (c) He, Q.; Liu, Z.; Xiao, P.; Liang, R.; He, N.; Lu, Z. *Langmuir* **2003**, *19*, 6982.
- (25) (a) Powell, H. M.; Lannutti, J. J. *Langmuir* **2003**, *19*, 9071. (b) Taguchi, K.; Ueguchi, T.; Ikeda, M. *Jpn. J. Appl. Phys.* **2000**, *39*, 5358.
- (26) (a) Nositschka, W. A.; Beneking, C.; Voigt, O.; Kurz, H. *Sol. Energy Mater. Sol. Cells* **2003**, *76*, 155. (b) Tada, T.; Hamoudi, A.; Kanayama, T.; Koga, K. *Appl. Phys. Lett.* **1997**, *70*, 2538.
- (27) Matsushita, S. I.; Yagi, Y.; Fujishima, A. *Chem. Lett.* **2002**, 524.

- (28) Velikov, K. P.; Christova, C. G.; Dullens, R. P. A.; van Blaaderen, A. *Science* **2002**, *296*, 106.
- (29) Lu, Y.; El-asser, M. S.; Vanderhoff, J. W. *J. Polym. Sci. B* **1998**, *26*, 1187.
- (30) Yi, G. R.; Moon, J. H.; Yang, S.-M. *Chem. Mater.* **2001**, *13*, 2163.

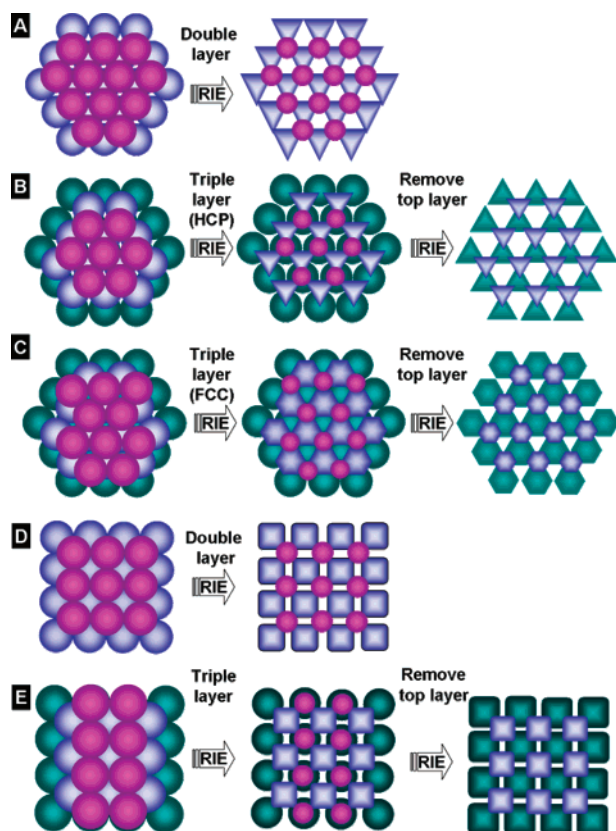


Figure 1. Schematic of CL for the fabrication of binary and ternary particle arrays with nonspherical building blocks. The upper layer in the colloidal layer acted as a mask for the lower layer; during anisotropic RIE the upper layer was etched more than the lower layer, resulting in binary (or ternary) particle arrays with patterned structures.

enhance hydrophilicity. The lift-up speed of the substrate was precisely controlled by an automated step-motor (Sigma Koki, SGSP2-85) and a controller (Sigma Koki, Mark-202). This device generated 10 steps of the lift-up speed starting from $0.025 \mu\text{m/s}$ to $2.0 \mu\text{m/s}$. The lift-up speed should remain as low as possible for the good ordered arrangement of a colloidal layer.

The thickness of the particle arrays can be controlled usually by adjusting the particle loading, lift rate, and evaporation rate; as the solvent evaporates after the monodisperse colloidal suspensions are dip-coated, capillary forces draw the particles, and the spherical particles self-organize to assemble ordered colloidal arrays.^{6,31} In our experiment, the evaporation rate remained almost constant because the experiments were performed at room temperature, and the lift-up speed was kept between $0.2 \mu\text{m/s}$ and $0.5 \mu\text{m/s}$. Under these conditions, the colloidal layers showed good ordered structures and the number of the arrayed particle layers was mainly controlled by adjusting the particle loading. As the particle loading increased, the number of colloidal layers increased. For a given particle loading, the dip-coating produced a colloidal assembly of a dominant structure with a specific number of particle layers. However, some voids and mixed multiple layers of single, double, and higher order layers appeared locally in the dip-coating process due to surface defects such as larger particles and impurities, stacking faults, and crystal defects.³¹ Experimental result for the relationship between the particle loading and the number of colloidal layers is shown in Table S1 of the Supporting Information.

For anisotropic partial etching of colloidal particles, RIE with plasma was performed directly onto preformed, well-ordered colloidal particle arrays with an RIE apparatus (VSR1E-400A, Vacuum Sciences). Except for the experiments in which varying RIE conditions were specified in

the text, the RIE proceeded with a gas mixture of CF_4 (40 sccm) and O_2 (60 sccm) at a pressure of 80 mTorr and a power density of 80 W. The RIE conditions were sufficiently gentle for partial etching of colloidal particles, without disturbing the ordered structure. In the RIE process, the upper layer of the colloidal particle arrays acted as a mask for the lower layer as a result of relative shadowing. During the anisotropic RIE, the upper layer was etched more than the lower layer, resulting in binary (or ternary) particle arrays with a patterned structure. At this step, the reactive plasma was easily diffused into the voids of the interstices between the particles, and it etched more severely around the voids. The morphology was observed by SEM (Philips-XL20SFEG).

Results and Discussion

Colloidal spheres can produce fcc and hcp crystal structures, which differ in the stacking of the hexagonally close-packed (111) layers.³² In the fcc structure, the sequence of stacked layers alternates as “ABCABC...”, while, in the hcp structure, the stacking sequence is “ABABAB...” stacking. Of the two crystal structures, the fcc structure is thermodynamically more stable than the hcp structure.^{32,33} A random hexagonal close packing (rhcp) structure, however, which is a mixture of the hcp and fcc structures, is observed experimentally in the fabrication of colloidal crystals under normal gravity. This phenomenon occurs because the free-energy difference between the two phases is very small, though the fcc phase is favored over the hcp phase.³²

Figure 1A shows the fabrication scheme of binary particle arrays from a double layer of spherical particles with a hexagonal arrangement. Figure 1B shows the ternary particle arrays from a triple layer of spherical particles with hcp arrangement. The scheme of Figure 1C shows the fabrication method of the ternary particle arrays from a triple layer of spherical particles with an fcc order. The formation of different patterns in hcp and fcc symmetry is possible because the interstitial spaces for plasma etching are different, as shown in Figure 1B and C. In the schemes of Figure 1B and C, a binary double layer can be created by completely etching out the top layer from the corresponding original triple layer.

Figure 1D and E display the schematics of CL when the (100) plane of an fcc colloidal crystal is exposed to an etchant flow. In this case, the pattern of the nonspherical particle arrays created by anisotropic etching is expected to differ from the previous case in which the (111) plane was exposed to the etchant flow. Colloidal crystals are likely to grow in the (100) direction when there is a confined geometry such as microchannels, V-shaped grooves, or inverse pyramid patterns.³⁴ Specifically, a (100)-oriented crystal structure in the V-groove can be formed by controlling the pitch and height of the V-groove and the diameter of the colloidal particles.^{34a}

In Figure 2A to D, double-layered arrays of binary particles with a “rounded” tetrahedral shape were produced after anisotropic RIE of the double layer of $1.01 \mu\text{m}$ PS spheres, which were arranged into a hexagonal structure. Under these conditions, the top layer was etched more than the lower layer because of relative shadowing. In Figure 2A, the average particle size of the top layer was about two-thirds of that of the original layer. When further RIE was performed, the particle size of the top layer became smaller and the particles of the bottom layer

(32) Pronk, S.; Frenkel, D. *J. Chem. Phys.* **1999**, *110*, 4589.

(33) Bolhuis, P. B.; Frenkel, D.; Mau, S.; Huse, D. *Nature* **1997**, *388*, 235.

(34) (a) Yin, Y.; Xia, Y. *J. Am. Chem. Soc.* **2003**, *125*, 2048. (b) Yin, Y.; Xia, Y. *Adv. Mater.* **2002**, *14*, 605. (c) Choi, D.-G.; Yu, H. K.; Jang, S. G.; Yang, S.-M. *Chem. Mater.* **2003**, *15*, 4169.

(31) Dimitrov, S.; Nagayama, K. *Langmuir* **1996**, *12*, 1303.

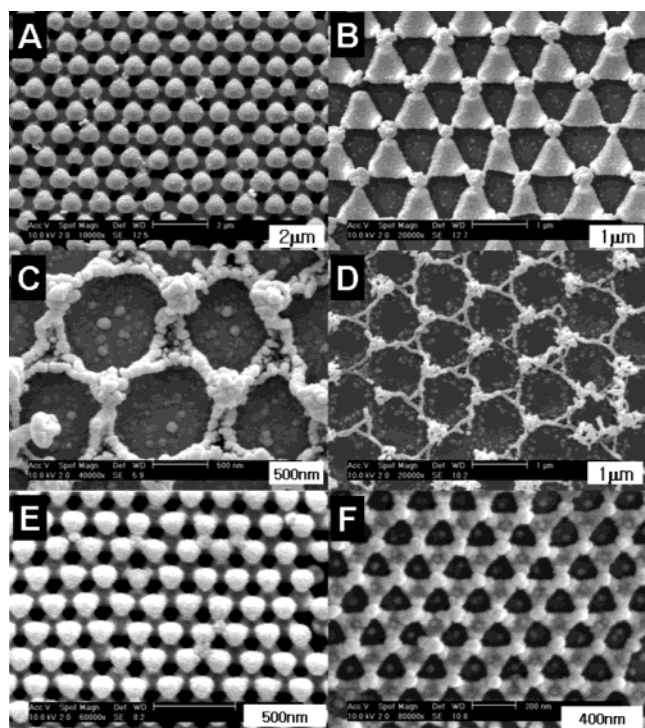


Figure 2. SEM images of particle arrays with nonspherical building blocks from a double layer with a self-assembled hexagonal arrangement. (A–D) Binary particle arrays and 2-D nanopatterns produced from a double layer of 1.01 μm PS beads. The exposure times to RIE were 4, 6, 8, and 12 min, respectively. (E and F) Binary particle arrays and 2-D nanopatterns produced from a double layer of small PS beads (200 nm). The exposure times to RIE were 1 and 1.5 min, respectively.

were severely etched. Finally, a triangular 2-D structure like the Star of David (Figure 2D) was formed. In Figure 2E and F, a double layer of 200 nm PS beads was etched to form binary

particle arrays. The resulting shape of the etched colloidal particles differs noticeably from the nonspherical particles produced by other techniques.^{7–10} The shape of the particles is quite complicated because the 3-D profile of the particle is given as a shadow image of the upper layer. Detailed images of 3-D shape are shown in cross-sectional SEM images (see Figure S1 of the Supporting Information).

Our method can be extended to ternary particle arrays from a triple layer of spherical PS beads arranged hexagonally, as shown in Figure 3. A close-packed triple layer array has either hcp symmetry (“ABA” particle array) or fcc symmetry (“ABC” particle array). Figure 3A shows ternary particle arrays, and Figure 3B shows binary particle arrays, all of which were produced from spherical PS bead arrays in hcp symmetry. To produce the double-layered arrays of Figure 3B, the top of the triple PS bead layers was removed by RIE for 2 min. We also produced ternary and binary particle arrays from the PS bead arrays in fcc symmetry. The results of the ternary particle arrays are shown in Figure 3C, and the results of the binary particle arrays are shown in Figure 3D.

The interstitial structures and spaces for plasma etching differ in hcp and fcc packings, as do the particle shapes and arrangements created by anisotropic RIE. As shown in Figure 3C, the bottom layer of the fcc structure had a more rounded hexagonal shape and the central parts were more severely etched than those of the hcp structure because of the relative shadowing difference. In the case of Figure 3D, the rounded hexagonal shape can be obtained for similar reasons as those given for Figure 3C. The top layer and second layer can be removed by further etching, resulting in a monolayer or other 2-D patterns (see Figure S2 of the Supporting Information).

Controlling the crystal phase is important for producing colloidal crystals with less stacking faults. Therefore, the

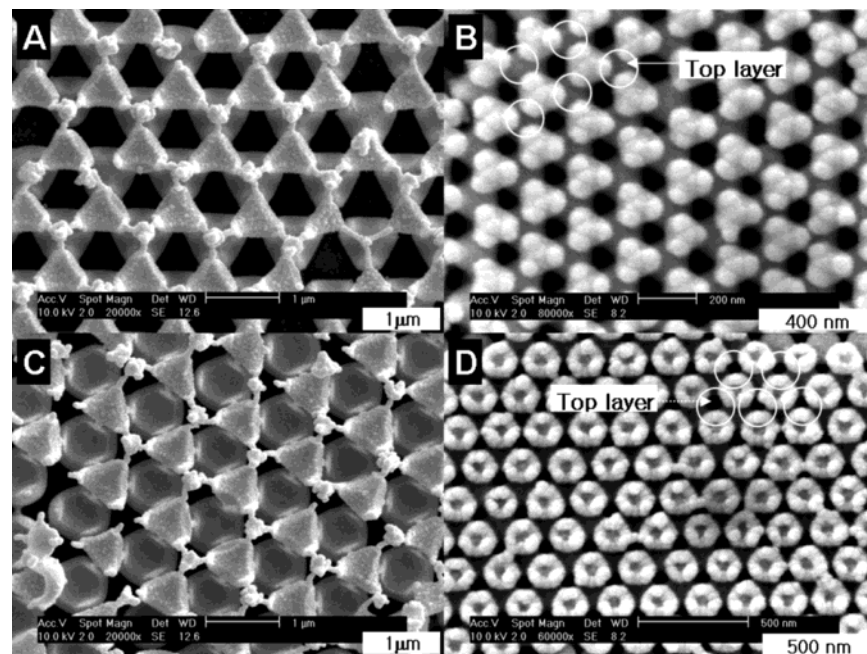


Figure 3. SEM images of ternary and binary particle arrays with nonspherical building blocks from a triple layer with a hexagonal arrangement. (A and B) Ternary and binary particle arrays produced from spherical PS bead arrays in hcp symmetry. (A) A ternary particle array produced after partial RIE etching of the PS bead (1.01 μm) array. The exposure time to RIE was 6 min. (B) A binary particle array produced after removing the top layer of the triple PS bead (200 nm) array. The exposure time to RIE was 2 min. (C and D) Ternary and binary particle arrays produced from spherical PS bead arrays in fcc symmetry. (C) Ternary particle arrays produced after partial RIE etching of PS beads (1.01 μm). The exposure time to RIE was 6 min. (D) A binary particle array produced after removing the top layer of the triple PS bead (200 nm) array. The exposure time to RIE was 2 min.

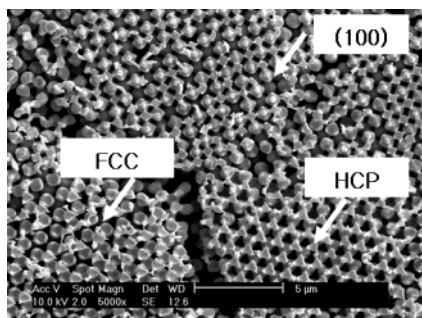


Figure 4. Observation of the crystal structure from a direct in-plane SEM image. The structure was formed with $1.01 \mu\text{m}$ PS spheres. The RIE time was 6 min.

manufacture of a pure fcc phase rather than a mixed fcc–hcp phase is needed to decrease the plane stacking faults. Several sophisticated methods have been developed to fabricate a pure fcc phase.^{35–38} If the meniscus at the air–water interface in dip-coating is slowly swept across a substrate by solvent evaporation, the fcc phase is more favorable and a colloidal structure with less defects can be fabricated.^{36,39} Recently, the transformation from a hcp to an fcc structure of colloidal spheres larger than 400 nm has been enhanced by applying a thermal convective flow to the solution via a temperature gradient to minimize sedimentation.³⁶ In some cases, raising the temperature of the solution³⁷ and shear-induced alignment³⁸ were attempted for the same purpose. From this point of view, the exact assessment of whether a crystal structure is an fcc or a hcp structure is an important issue in the research of colloidal science.⁴⁰ However, determining the exact characterization of the fcc and hcp crystal structures is generally difficult from simple and direct SEM images. This problem is due to the difficulty of determining the exact angle between fcc and hcp structures from cross-sectional SEM images. As a result, estimating which crystal face is shown is also difficult.⁴⁰ By using RIE, our method enables us to easily show the crystal structure from a direct in-plane SEM image as shown in Figure 4.

We also prepared a 2-D colloidal monolayer of PS beads of $1.01 \mu\text{m}$ by controlled dip-coating to create RIE-induced patterns. As shown in Figure 5A, the diameter of polystyrene particles was gradually reduced with an increase of RIE time. A similar technique for the formation of a size-controllable nanostructure array has been developed using PS beads whose diameters could be arbitrarily reduced by RIE with oxygen.⁴¹ In the present study, however, structures with “hexagonally networked protrusions” appeared when the exposure time to RIE with O_2 and CF_4 plasma exceeded 6 min (Figure 5B). Similar polygonal patterns were observed when thin PS films prepared on silicon wafers dewet spontaneously above the glass transition temperature.⁴² Recently, Powell and Lannutti conducted a comprehensive study on the formation mechanism of the

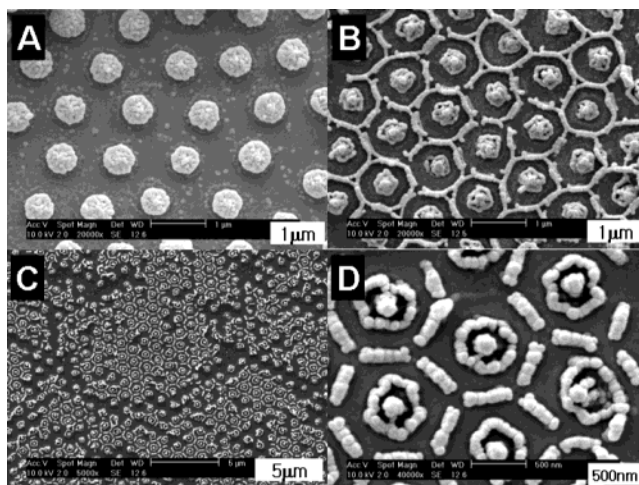


Figure 5. SEM images of particle arrays from a colloidal monolayer of PS beads ($1.01 \mu\text{m}$). The exposure time to RIE was (A) 4 min, (B) 6 min, (C) 12 min, and (D) 12 min. Images C and D differ in magnification.

polygonal structure produced by RIE of poly(ethylene terephthalate) (PET) film with various compositions of reactive plasmas.^{25a} In their case, the PET film was unsupported and initially a single phase material. Exposure to reactive plasma produced relatively polar low-molecular-weight fragments via chain scission of PET, as well as increased temperature. Therefore, the PET film was exposed to reactive plasma, producing a two-phase material, i.e., a thin mobile surface of polar low-molecular-weight fragments over an immobile apolar PET surface.^{25a} Various types of patterns including polygonal protrusions and nanofibrillar surface were eventually formed because of the dewetting phenomena between the polar surface and the apolar substrate. The final surface morphology depended strongly on the gas compositions and RIE conditions, which influenced the chain scission and temperature increment.^{25a}

In this work, we used a mixture of O_2 and CF_4 as reactive ion source to etch close-packed PS beads on a glass substrate instead of continuous polymer film. As observed in the previous study on the PET film,^{25a} exposure to RIE plasma not only broke the PS chains to produce polar low-molecular-weight fragments but increased the surface temperature. In particular, O_2 and CF_4 , when mixed together for use in plasma etching, create the oxyfluoride ion, which is a highly reactive etching agent for polymeric substances. This ion is particularly adept at cutting the carbon–carbon bonds in the polymer backbone.^{43a} Moreover, although pure CF_4 plasma etches silicon oxide slowly, the presence of O_2 will increase the fluorine free radical concentration and increase the etching rate of silicon oxide.^{43b} Consequently, use of O_2 – CF_4 mixture plasma not only reduces the wettability of the glass surface by the preferential fluorination of silicon oxide but also increases the surface temperature. As shown in Figure 5A, in the early stage of RIE, using O_2 – CF_4 mixture plasma, the diameter of the PS beads was reduced, and the reduced PS beads were flattened on the substrates. With an increase of RIE time above 6 min, however, the hexagonally networked protrusions around the flattened spheroidal dots were created as shown in Figure 5B to D. As we shall see shortly in

(35) van Blaaderen, A.; Ruel, R.; Wiltzuis, P. *Nature* **1997**, *385*, 321.

(36) Vlasov, Y. A.; Bo, X.-Z.; Sturm, J. C.; Norris, D. J. *Nature* **2001**, *414*, 289.

(37) Im, S. H.; Park, O. O. *Langmuir* **2002**, *18*, 9642.

(38) Amos, R. M.; Rarity, J. G.; Tapster, P. R.; Shepherd, T. J. *Phys. Rev. E* **2000**, *61*, 2929.

(39) (a) Zhu, J.; Li, M.; Rogers, R.; Meyer, W.; Ottewill, R. H.; Russel, W. B.; Chaikin, P. M. *Nature* **1997**, *387*, 883. (b) Vlasov, Y. A.; Astratov, V. N.; Baryshev, A. V.; Kaplyanskii, A. A.; Karimov, O. Z.; Limonov, M. F. *Phys. Rev. E* **2000**, *61*, 5784.

(40) Jiang, P.; Bertone, J. F.; Hwang, K. S.; Colvin, V. L. *Chem. Mater.* **1999**, *11*, 2132.

(41) Haginoya, C.; Ishibashi, M.; Koike, K. *Appl. Phys. Lett.* **1997**, *71*, 2934.

(42) Sharma, A.; Reiter, G. *J. Colloid Interface Sci.* **1996**, *178*, 383.

(43) (a) Kogoma, M.; Kasai, H.; Takahashi, K.; Moriwaki, T.; Okazaki, S. *J. Phys. D: Appl. Phys.* **1987**, *20*, 147. (b) Min, J.-H.; Hwang, S.-W.; Lee, G.-R.; Moon, S. H. *J. Vac. Sci. Technol., A* **2003**, *21*, 1203.

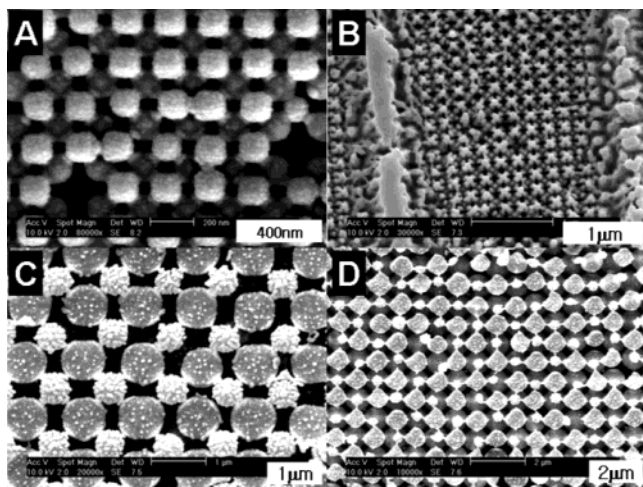


Figure 6. SEM images of binary and ternary particle arrays with nonspherical building blocks when the (100) plane was exposed to RIE. The PU substrate with patterned grooves was fabricated by replica molding with a V-shaped diffraction grating. The angle between the edges of the V-shaped groove was 70° . Nonspherical binary particle arrays produced from a double layer of PS beads of 200 nm (A) and $1.01 \mu\text{m}$ (C). (B) SEM images at lower resolution for nonspherical particle arrays of 200 nm particle arrays with the (100) plane facing to the etchant flow within the V-shape groove. (D) Nonspherical ternary particle arrays produced from a triple layer of $1.01 \mu\text{m}$ PS beads with the (100) plane normal to the etchant flow. The RIE exposure times were 1 min for the 200 nm PS beads and 6 min for the $1.01 \mu\text{m}$ PS beads.

Figure 7A to E, the RIE with pure O_2 plasma alone did not produce the polygonal protrusions. Moreover, thermal annealing above glass transition temperature without the RIE process was not able to produce the polygonal protrusions and simply made the PS beads sintered together without reducing particle size (see Figure S3 of the Supporting Information). Therefore, these patterned protrusions were also induced by Rayleigh instability arising in such a way that the unremoved polar low-molecular-weight fragments produced by the RIE process spontaneously dewet the fluorinated glass surface.^{25a,42,43} The Rayleigh instability was also facilitated due to the viscosity reduction and the temperature increment both caused by $\text{O}_2\text{-CF}_4$ mixture plasma. After sufficient exposure to RIE to induce spontaneous dewetting, novel polygonal patterns such as a hexagonal network with flattened spheroidal dots in the center were formed, as shown in Figure 5C and D.

As mentioned earlier, we prepared multilayered PS bead arrays using replica-molded PU substrates with V-shaped grooves. Owing to the confined geometry of the V-shaped groove, the (100) plane was parallel to the substrate and normal to the etchant flow. We expected the prepared patterns and particle shapes to differ significantly from the results shown in Figures 2 and 3, in which the etchant flow was directed toward the (111) plane. The SEM images of Figure 6A and B show the resulting nonspherical rectangular particle arrays prepared from 200 nm PS beads with the (100) plane facing to the etchant flow. Indeed, the shape and arrangement of the etched PS particles were distinctively different from the previous cases with the (111) plane normal to the etchant flow. Binary and ternary particle arrays with rectangular structure were also produced by using double and triple layers of $1.01 \mu\text{m}$ PS beads, respectively; the results are reproduced in Figure 6C and D.

As shown in Figure 1D and Figure 6, the rectangular interstices were enlarged when the upper layer of the particle

arrays was partially etched. The reactive plasma then easily diffused into the interstices. Further RIE resulted in the structure of Figure 6.

In a few recent studies, pure O_2 plasma has been used for the fabrication and size control of colloidal patterns, though these studies were limited to colloidal monolayers and double layers.^{26,27} Here, we extended these results to colloidal multilayers with different orientations. Figure 7 shows the SEM images of 2-D or 3-D arrayed patterns produced from colloidal multilayers when the (111) planes were exposed toward a pure O_2 plasma. The RIE conditions were exactly the same as those of previous results except that pure O_2 (60 sccm) was used instead of a gas mixture of CF_4 and O_2 . The results of the monolayer (Figure 7A to C) and the double layer (Figure 7D and E) are similar to those of other researchers.^{26,27} The particle size was reduced with RIE time without forming the kind of polygonal patterns seen in Figure 5, which were produced by RIE with a gas mixture of CF_4 and O_2 . The sizes of the interstices in the double layer can be tuned by RIE conditions. In Figure 7D and E, the sizes of the interstices of a close-packed colloidal double layer of $1.01 \mu\text{m}$ PS particles increased from 160 nm to a range of 450 nm to 600 nm with RIE time. As shown in Figure 7E, the central part of each PS bead in the bottom layer was severely etched because of RIE etching through the voids of the interstices, and the particles of the bottom layer were then divided into three parts.

Novel “flower shape” patterns (Figure 7F) were fabricated when further RIE was performed on the pattern shown in Figure 7E. These patterns were induced because the thin central parts of the bottom layer, which have a polygonal shape, were completely removed before the top layer was removed by further RIE (see Figure S4A). This approach was extended to a triple layer, as shown in Figure 7G–L. A different pattern (Figure 7G) that could be described as “a dog’s paw morphology” was formed using a triple layer with hcp (“ABA”) symmetry. The experimental conditions of Figure 7G were identical to those of Figure 7F. As a second layer was removed by further RIE, the flower-shaped patterns similar to those in Figure 7F were obtained from a triple layer (Figure 7I).

We also produced different patterns from a triple layer with fcc (“ABC”) symmetry. The results are shown in Figure 7J and K. The RIE exposure time of Figure 7J was the same as that of Figure 7G. Patterns described as a “donut with a triangular hole” were produced by further RIE (Figure 7K). The formation of different patterns in hcp and fcc symmetry is due to the different interstitial structures into which plasma flows when the colloidal layer is exposed to RIE. Figure 7L shows the results of using a quadruple layer (“ABCA” symmetry). In Figure S4 of the Supporting Information, we included SEM images of situations in which either a (100) plane of a triple layer with fcc symmetry was exposed to O_2 plasma or a (111) plane of a quadruple layer of hcp (“ABAB”) symmetry was exposed to O_2 plasma.

Finally, we investigated the effect of thermal annealing of the PS colloidal arrays on the RIE-induced surface morphology. In doing this, double-layered PS beads were annealed above glass transition temperature prior to exposure to reactive ions. As the annealing time increased, sintering occurred between slightly flattened particles because of the increased polymer mobility at the high temperature. Then, the annealed particle array on the glass substrate was exposed to reactive plasma

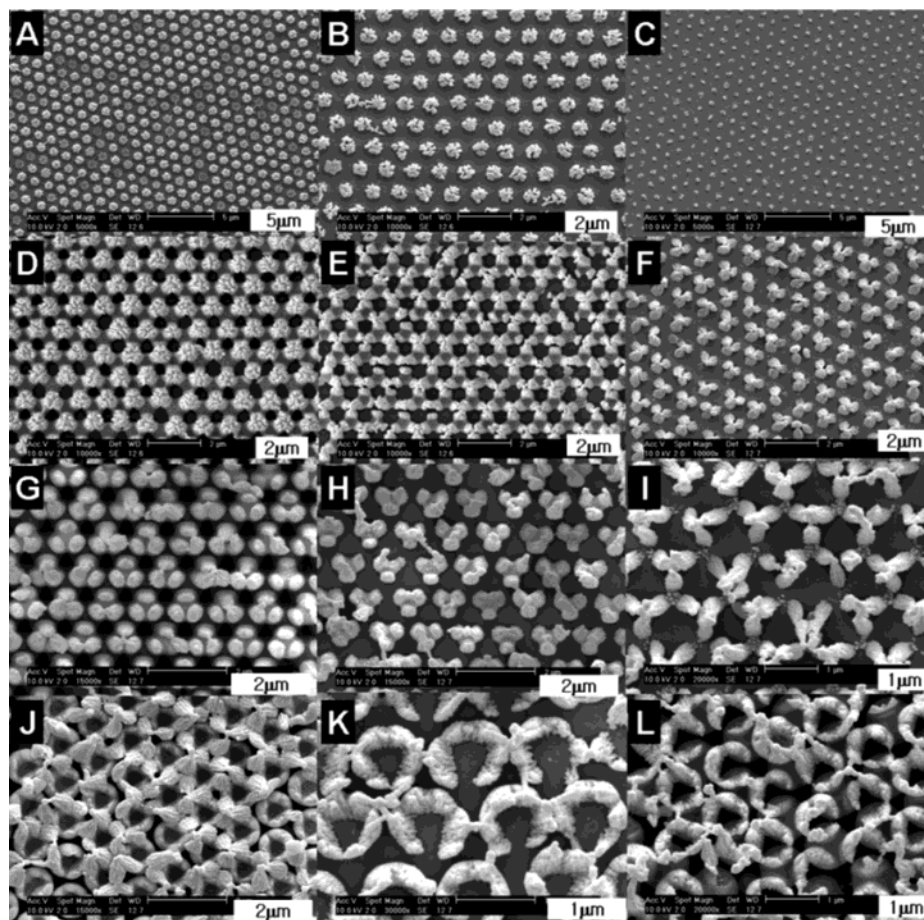


Figure 7. SEM images of 2-D or 3-D arrayed patterns produced from colloidal multilayers when pure O_2 RIE was used. (A–C) Patterns produced from a monolayer of PS particles. The exposure time to RIE was (A) 4 min, (B) 6 min, and (C) 8 min, respectively. (D–F) Patterns produced from a double layer. The exposure time to RIE was (D) 4 min, (E) 6 min, and (F) 8 min, respectively. (G–I) Patterns produced from a multiple layer of PS particles with a hcp structure (“ABA” symmetry) (G–I) and an fcc structure (“ABC” symmetry) (J–L). The exposure time to RIE was (G) 8 min, (H) 10 min, (I) 12 min, (J) 8 min, (K) 10 min, and (L) 10 min, respectively.

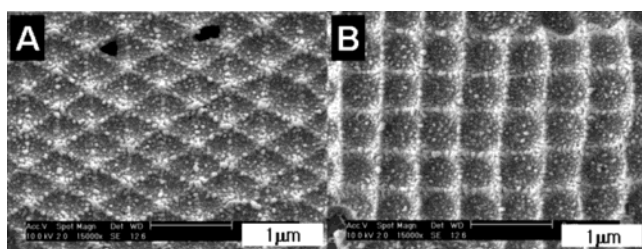


Figure 8. SEM images of 2-D arrayed patterns produced by RIE of colloidal double layers of PS beads ($1.01 \mu\text{m}$) after annealing at 120°C for 30 min. The exposure time to RIE was 6 min. (A) Patterns produced when the (111) plane faced the etchant flow. (B) Patterns produced when the (100) plane was normal to the etchant flow.

mixtures of CF_4 and O_2 . Figure 8 shows the intermediate structures of the annealed film when exposed to RIE. As noted, the surface morphology looked like a polymer film with patterned protrusions. The hexagonal and square patterns shown in Figure 8 were obtained by controlling the orientation of PS bead layers.

Conclusions

We have demonstrated a new, easy approach to the fabrication of nonspherical colloidal particle arrays with a long-range order from self-organized spherical colloidal layers that acted as masks in anisotropic RIE. The resulting patterns and particle shapes

were dependent on the crystal orientation relative to the substrate, the number of colloidal layers, and the RIE conditions. The structures produced by anisotropic RIE can lead to the creation of new types of 2-D nanopatterns or 3-D colloidal particle arrays. In principle, our approach can be extended to quadruple (or higher order) layers to create more complicated structures that cannot otherwise be produced. We have also demonstrated that, by using RIE, CL is a versatile and useful technique in the field of nanopattern fabrication. The resulting structures of nonspherical building blocks can be used as templates or masks for microscale or nanoscale 2-D patterning or 3-D layered colloidal crystals.

Acknowledgment. This work was supported by the Center for Nanoscale Mechatronics and Manufacturing of the 21st Century Frontier Research Program (M102KN010001-02K1401-00212) and the National R&D Project for Nano Science and Technology. The authors also acknowledge partial supports from the Brain Korea 21 program, CUPS-ERC and the IMT-2000 Projects.

Supporting Information Available: SEM images of more detailed explanation about 3-D structure and explanation of structure formation. See Figures S1–S4. This material is available free of charge via the Internet at <http://pubs.acs.org>.

JA0319083